Clays and Clay Minerals, Vol. 38, No. 1, 1–13, 1990.

HIGH-RESOLUTION TRANSMISSION ELECTRON MICROSCOPY AND ELECTRON DIFFRACTION OF MIXED-LAYER ILLITE/SMECTITE: EXPERIMENTAL RESULTS

DAVID R. VEBLEN, GEORGE D. GUTHRIE, JR., KENNETH J. T. LIVI
Department of Earth & Planetary Sciences, The Johns Hopkins University
Baltimore, Maryland 21218

AND

ROBERT C. REYNOLDS, JR.
Department of Geology, Dartmouth College, Hanover, New Hampshire 03755

Abstract—High-resolution transmission electron microscopy (HRTEM) and electron diffraction experiments have been performed on R1 and R>1 illite/smectite (I/S) samples that from X-ray powder diffraction (XRD) experiments appear to contain well-ordered layer sequences. The HRTEM images confirmed earlier computer image simulations, which suggested that periodicities due to I/S ordering can be imaged in TEM instruments of moderate resolution. The experiments also confirmed that in instruments of this sort, the strongest contrast arising from the compositional difference between I and S layers occurs under rather unusual imaging conditions of strong overfocus. Some selected-area electron diffraction (SAD) patterns showed additional diffraction spots consistent with R1 and R3 ordering. SAD patterns and cross-fringes arising in HRTEM images from non-00*l* reciprocal lattice rows indicated that the stacking vectors of most adjacent 2:1 layers were not randomly oriented with respect to each other. Thus, the I/S was not fully turbostratic, but instead consisted of very thin, coherently stacked crystallites that extended across the fundamental particles postulated by Nadeau and coworkers.

S/(I + S) ratios were determined for about seventy HRTEM images obtained and interpreted by three different TEM operators. These ratios were consistent with those obtained from standard XRD procedures, suggesting that results obtained by XRD can be used to infer the initial structural state of mixed-layer I/S prior to treatment of samples for XRD experiments. The HRTEM experiments thus demonstrated that the two specimens examined consisted of ordered I/S existing as small crystals, most of which contained more layers than the fundamental particles of Nadeau and coworkers. The non-turbostratic stacking suggests an energetic interaction between the individual fundamental particles, leading to at least two alternative thermodynamic descriptions of these materials. Although the I/S crystals in the present experiments probably were disaggregated into fundamental particles during sample preparation for XRD, the I/S crystals appear to have separated only along the smectite interlayers. If the term "fundamental particle" is to be used for primary, untreated I/S, its original definition should be modified to include not only free particles, but also those that occur as layers within small crystals. It further should be recognized that these particles can interact thermodynamically and crystallographically with their neighbors.

Key Words—Electron diffraction, Fundamental particle, High-resolution transmission electron microscopy, Illite/smectite, Interstratification, Smectite.

INTRODUCTION

Previously, Guthrie and Veblen (1989a, 1989b, 1989c) used computer simulations to show how high-resolution transmission electron microscopy (HRTEM) images of mixed-layer illite/smectite (I/S) can be expected to vary as a function of various experimental parameters. They showed that it is, indeed, theoretically possible to image the ordering of illite and smectite interlayers in untreated samples in which the layer spacings are collapsed to a uniform 10 Å in the vacuum of the electron microscope (Guthrie and Veblen, 1989a), as well as in samples in which the smectite interlayers are expanded (Guthrie and Veblen, 1989c). In addition, they delineated certain experimental conditions under which contrast due to I/S ordering is maximized. These computer simulations were performed primarily for transmission electron microscopes of moderate resolution, because such instruments are readily available to clay mineralogists in dozens of institutions, whereas access to dedicated ultra-high-resolution instruments is limited.

The fact that computer image simulations are essential for the reliable interpretation of HRTEM data is underscored by the fact that Guthrie and Veblen's (1989a) work has already spurred the reevaluation of previously published reports on I/S (for references to several papers in this field, see Guthrie and Veblen,

Copyright © 1990, The Clay Minerals Society

https://doi.org/10.1346/CCMN.1990.0380101 Published online by Cambridge University Press

Table 1. Electron microprobe analyses of the illite/smectite samples (wt %).

	R1		R>1	
SiO_2	47.74		47.29	
Al_2O_3	24.78		29.58	
TiO_2	0.18		0.07	
FeO	2.04		0.10	
MgO	4.01		1.95	
MnO	0.04		0.02	
CaO	0.62		0.66	
Na_2O	0.13		0.00	
K_2O	4.66		7.67	
Total	84.20		87.34	
Mineral formulae (11 oxygens):				
Si	3.48	4.00	3.34	4.00
Al^{IV}	0.52		0.66	
Al^{VI}	1.61	2.18	1.81	2.03
Ti	0.01		0.00	
Fe	0.12		0.01	
Mg	0.44		0.21	
Mn	0.00		0.00	
Ca	0.05	0.50	0.05	0.74
Na	0.02		0.00	
K	0.43		0.69	
Σ_{cat}	6.68		6.77	

1989a). For example, Ahn and Peacor (1989) have reinterpreted their earlier work on I/S in Gulf Coast shales (Ahn and Peacor, 1986a); I/S in which order was not observed is now recognized to be ordered, in agreement with powder X-ray diffraction (XRD) results on the same samples. In addition, in a study complementary to the present one, Ahn and Buseck (1990) used image simulations and data from an ultra-high-resolution TEM instrument to determine stacking sequences in several I/S samples.

In the present paper, we have applied our computer simulation results to the experimental imaging of two essentially pure I/S specimens that exhibited exceptionally good R1 and R>1 ordering in XRD experiments; preliminary reports of this work, as well as more general comments on the HRTEM imaging of sheet silicates, were given by Guthrie and Veblen (1988, 1989b, 1989c). The present paper is intended to answer the following questions: (1) Under fortuitous conditions, can HRTEM images obtained with instruments of moderate resolution be used to obtain the exact sequence of I and S layers? (2) Are the ratios of I and S layers obtained by counting the layers on HRTEM images consistent with the ratios obtained from XRD? (3) In the specimens used for this study, do packets or small crystals of ordered I/S (either R1 or R>1) exist in the bulk material prior to preparation for XRD studies? (4) If ordered packets do occur in the bulk, untreated material, can electron diffraction patterns be obtained that confirm the periodicity of the ordering? (5) In addition to the ordering of I and S layers, are the layer stacking vectors of adjacent 2:1 layers crystallographically related to each other, i.e., is the stacking coherent, or is the I/S turbostratic?

For much of the discussion below, a working definition is needed of what an I/S crystal is. An I/S crystal or crystallite for the purposes of this paper is defined as a group of 2:1 layers that contains illite (or nonexpandable) and smectite (or expandable) interlayers and that exhibits coherent (non-turbostratic) stacking. Such crystals can possess stacking disorder, just as in micas; however, we differentiate between such disordered crystals and turbostratically stacked packets of layers. Such packets of I/S that are not coherently stacked (i.e., that contain stacking rotations other than mod 60°) might be considered to be one-dimensional crystals, but in this paper they are simply called packets, not crystals.

SAMPLE DESCRIPTION AND EXPERIMENTAL METHODS

Specimens

The two I/S samples used for this study are from Japan (JHS-WS-10-199.9) and Zempleni, Hungary, henceforth referred to as samples R1 and R>1. The Japanese sample is hydrothermally altered volcanic rock from the Shinzan Area, Akita Prefecture, northeast Japan. It was described by Inoue and Utada (1983) and Inoue *et al.* (1978). The sample was provided to us by A. Inoue. The R>1 I/S is also a hydrothermal occurrence; the sample was provided by J. Środoń. The two specimens were selected for study because they are well-ordered, they occur as coherent aggregates that can be cut into petrographic thin sections for ion milling, and they are both very pure I/S. Thus, we were able to compare directly the X-ray and electron microscopy results, avoiding ambiguities that are inherent in studies of impure specimens, such as shales. In such studies of rocks, XRD typically is performed on clay separates of specific size fractions, which may contain clay minerals other than I/S. Electron microscopy commonly is performed on unsorted bulk rock samples, which contain large amounts of additional minerals, and it is then difficult to know for certain which components in the ion-milled TEM specimen actually correspond to the material studied by XRD.

Both of the specimens examined here apparently had been thermally metamorphosed at low temperatures to produce the ordered illite/smectite structures. Average electron microprobe analyses (obtained at Johns Hopkins University using a JEOL 8600 Superprobe and silicate standards) are presented in Table 1. Although the totals for the analyses are slightly low (probably due to sample porosity and water content), the analyses indicated that both specimens were K-illite/smectite. The trends in interlayer occupancy and tetrahedral Al contents are consistent with the differences between the inferred proportions of illite in the R1 and R>1 samples. XRD studies of these specimens (per-

https://doi.org/10.1346/CCMN.1990.0380101 Published online by Cambridge University Press

formed at Dartmouth College) indicated that the R1 specimen contained 45% expandable layers, whereas the R>1 material contained 17% expandable layers. The techniques of XRD sample preparation, analysis, and data interpretation were detailed by Keller *et al.* (1986).

Electron microscopy

Specimens for electron microscopy were prepared by two methods. Some specimens were made by argon-ion milling discs cut from petrographic thin sections. The discs were coated lightly with noncrystalline carbon to render them conductive enough for TEM work. Observations on these specimens were made on the thin edges along holes produced during the ion milling process. Other specimens were prepared by light crushing in ultrapure water and evaporating drops of the suspension on holey carbon support films. These specimens were observed mainly in areas in which clay particles were wrapped around holes in the support film. Where a particle wraps around a hole, the layers of the structure are parallel to the electron beam for a short distance, and lattice images showing the basal spacing can be obtained. Similar results were obtained for both sample preparation methods, indicating that the configuration of the clay material was the same both before and after mild disaggregation of the bulk sample and therefore that the results were not merely an artefact of the preparation process.

Electron microscopy was performed (at Johns Hopkins) with a Philips 420 transmission electron microscope using both T and ST objective lenses. Details on instrumentation and operating parameters were described by Livi and Veblen (1987). In some experiments, the objective aperture diameter was chosen to match the point-to-point resolution of the TEM instrument. Other images were obtained with smaller objective apertures that permitted contributions only from the 00*l* reciprocal lattice row, thus suppressing potentially confusing cross-fringes arising from *hkl* rows. By observing the specimen while changing the microscope focus, contrast consistent with I/S ordering could best be seen at relatively large values of overfocus (e.g., $\Delta f \cong +1000$ Å); the computer simulations of Guthrie and Veblen (1989a, 1989b, 1989c) showed that this contrast can, indeed, arise from the ordering of illite and smectite layers. Although 4.5-Å cross-fringes formed by imaging *hkl* diffraction spots could be observed in some of these overfocused images, they were much clearer in images obtained at underfocused values near Scherzer focus. Thus, images having the clearest cross-fringes typically did not show the image modulations indicative of ordering of I and S layers.

Due to rapid beam damage and highly variable crystallographic orientation of the specimen, even over relatively small (micrometer scale) distances, it was difficult to orient the specimen in the standard way by tilting while observing the electron diffraction pattern. Furthermore, because the specimens consisted of very small (<1 μm thick), deformed crystals or packets of crystals in apparently random orientation, results were obtained more efficiently by two alternative methods: (1) One method consisted of moving across the specimen under HRTEM conditions and searching for areas that were close enough to proper orientation to show clear basal lattice fringes. If such areas were observed, the microscope was focused quickly, and the image was recorded immediately on film. (2) The other method consisted of tilting the specimen with the objective aperture inserted and observing when I/S flakes displayed the mottled dark contrast that is characteristic of sheet silicate crystals oriented with the layers approximately parallel to the electron beam. The magnification was then increased, and the image was focused and recorded on film as above.

Electron microscopy was performed by three different microscopists (D.R.V., K.J.T.L., and G.D.G.), and similar results were obtained by all three. As noted by other workers referenced in Guthrie and Veblen (1989a), however, I/S specimens are difficult materials to work with in the TEM; the majority of the area observed on most films does not contain much or any interpretable information on the sequences of I and S layers. This lack of information is consistent with the computer simulation results, which showed that I/S ordering should be apparent only under rather special conditions of crystal orientation, crystal thickness, and microscope focus. In addition, many images showed extensive beam damage and, hence, contained little useful information. Nevertheless, hundreds of films were recorded during this study and we therefore are confident that the observations accurately represent the structure of the two I/S specimens.

ELECTRON DIFFRACTION AND MICROSCOPY RESULTS

Electron diffraction

As noted above, well-oriented selected-area electron diffraction (SAD) patterns were difficult to obtain from the I/S specimens studied. Due to spherical aberration in the objective lens and restrictions on the practical aperture size, the minimum resolution of the SAD method for many electron microscopes is on the order of 0.5 μm (Hirsch *et al.*, 1977, p. 19), and much of the material had crystals thinner than that in the c^* direction. For such materials, convergent-beam electron diffraction commonly can be used in place of SAD, but rapid beam damage precluded the use of this method for I/S.

Diffraction results on layer sequences. Despite the difficulties, some reasonable SAD patterns containing c^* were obtained for each specimen by using a 30-μm selected-area aperture having a projected diameter on

https://doi.org/10.1346/CCMN.1990.0380101 Published online by Cambridge University Press

Table 2. Displacement of true area selected from apparent aperture position.

d (Å)	α (radians)	$C_s\alpha^3$ (Å)
20	0.00167	0.06
10	0.00334	0.45
5	0.00668	3.58
2.5	0.01336	28.62
1.25	0.02672	228.92

the specimen of 0.2 μm. The primary effect of spherical aberration on the resolution of SAD patterns is to displace the region from which diffraction information arises from the apparent selected-area aperture position by an amount $C_s\alpha^3$, where C_s is the spherical aberration coefficient of the objective lens and α is the angle between the diffracted beam and the central electron beam (Hirsch *et al.*, 1977, p. 19). To minimize this effect, we used a low-spherical-aberration objective lens (C_s = 1.2 mm). The displacement function for this lens is given in Table 2 for several d-values. Inasmuch as the displacement occurred in opposite directions for opposite sides of the SAD pattern, the resolution of the SAD experiments was therefore degraded by less than 500 Å out to a value of d = 1.25 Å. Combined with the projected aperture size, these data indicate that the SAD resolution was about 0.25 μm.

SAD patterns with c^* all showed relatively sharp 10-Å diffraction spots and higher orders corresponding to the basic 2:1 layer repeat. Between these substructure spots were either relatively intense streaking or additional diffraction spots. All SAD patterns containing c^* also contained additional diffraction rows parallel to c^* that commonly were heavily streaked. Streaking in the 00l rows conceivably could have resulted from multiple diffraction arising from these parallel rows, as has been noted for analogous streaking in the k = 3n rows of micas with substantial stacking disorder. In the present experiments, however, the streaking was more intense than that encountered in the 00l rows of disordered micas, and it probably arose from disordered sequences of illite and smectite layers, combined with the shape effect of very thin crystals. Radial streaking of the type observed is not consistent with variable orientation effects from small crystals (or aggregates of fundamental particles), which instead produce concentric streaking; such concentric streaking or arcuate diffraction spots were also observed frequently.

Most SAD patterns from the R1 specimen showed both streaking parallel to c^* and diffraction maxima consistent with 20-Å periodicity (Figure 1a). Although heavy streaking parallel to c^* predominated in the R>1 material, spots indicative of 40-Å periodicity also were noted (Figure 1b). The two patterns in Figures 1a and 1b are suggestive of relatively good . . .ISIS. . . and . . .ISIIISII. . . long-range ordering, respectively. In SAD

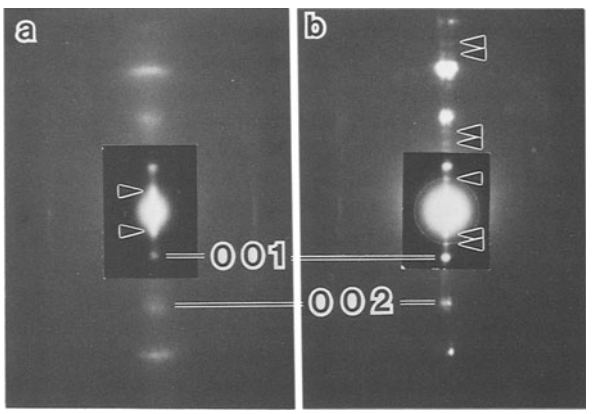


Figure 1. Selected-area electron diffraction patterns showing c^* for mixed-layer illite/smectite. Each pattern is a composite of two different print exposures in order to show more detail in both the central and outer portions. Indices of the 001 and 002 substructure reflections are indicated and are based on the 10-Å subcell. (a) Pattern showing intensity due to R1 ordering (arrowed). (b) Pattern showing intensity due to R3 ordering (arrowed). Sharp, fine circle near center of pattern is an artefact due to scattering from an aperture in the illumination system of the electron microscope.

patterns in which this doubling or quadrupling of the (001) periodicity was apparent in the 00l reciprocal lattice row, the same periodicities did not appear in the parallel rows with $k \neq 3n$, as has been noted for multiple-layer diffraction patterns arising from polytypism. The SAD patterns thus were consistent with ordering of I and S layers, rather than with the ordered stacking of identical layers. No evidence for ordered periodicities other than 40 Å were observed in the R>1 material.

Diffraction results on layer stacking. Additional SAD patterns obtained with various selected-area apertures and with the electron beam approximately normal to the I/S layers commonly showed complete or incomplete rings from diffraction by planes having indices (hk0), consistent with turbostratic stacking in the original, bulk specimens (Figure 2a). Such patterns, however, reflect the average structure over a relatively large specimen area. They typically are also averages from both thin and relatively thick regions of the specimen. Therefore, SAD experiments were performed near the edges of ion-milled specimens as described above, using a selected-area aperture with a projected diameter on the specimen of 0.2 μm and a low-spherical-aberration ST objective lens (to minimize degradation of SAD resolution by electron optical effects).

With this experimental configuration, both specimens commonly produced hexagonal SAD patterns characteristic of stacking order or stacking vector rotations of mod 60° (0°, ±60°, ±120°, and 180° only), or patterns with only a few such superimposed hexagonal patterns of differing intensity, implying that the

https://doi.org/10.1346/CCMN.1990.0380101 Published online by Cambridge University Press

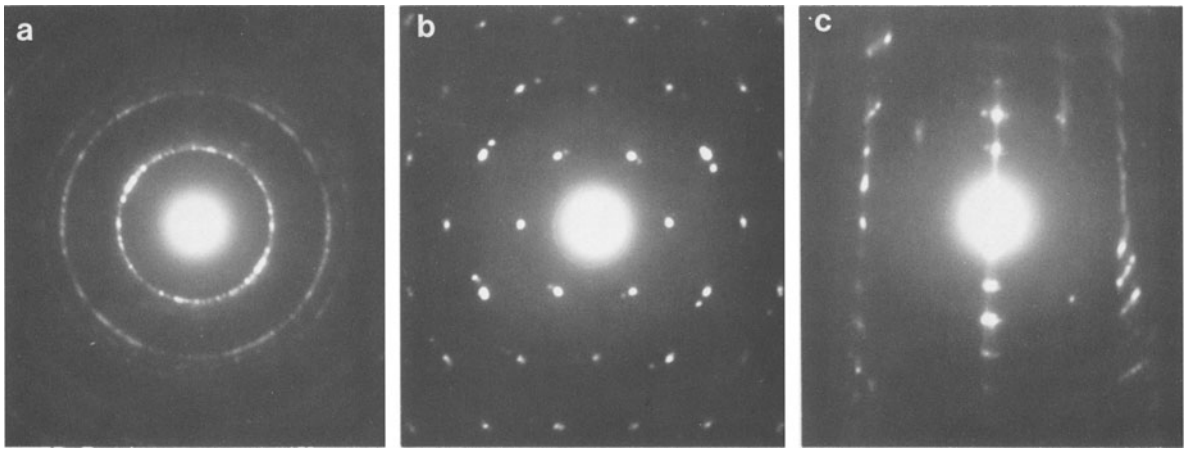


Figure 2. Selected-area electron diffraction patterns for R1 mixed-layer illite/smectite. (a) *hk*0 pattern showing apparent turbostratic structure. (b) *hk*0 pattern obtained from a smaller area and indicating non-turbostratic stacking. Three hexagonal sets of diffraction spots are present, each with different intensity, indicating that the pattern is from three coherently stacked crystals of different thickness. (c) Pattern showing discrete *hkl* diffraction spots.

pattern arose from a few coherently stacked crystals of differing thickness (Figure 2b). Because such patterns were obtained from wedge-shaped specimen areas that contained material thicker than an individual layer, at least a substantial portion of both samples possessed non-turbostratic stacking. Other specimen areas still produced incomplete *hk*0 ring patterns with this experimental configuration, but it was not clear from the SAD experiments alone whether these areas were truly turbostratic or whether these patterns were from relatively thick areas containing numerous overlapping thin crystallites having coherent layer stacking. Because specimen thickness is difficult to measure in the TEM, the thickness of the coherently stacked crystallites had to be determined by HRTEM imaging, as described below.

SAD patterns obtained with the electron beam parallel to the layers of the specimen commonly showed arcuate and/or highly streaked *hk* rows similar to those shown by Nadeau (1985, Figure 5), consistent with turbostratic stacking and/or bending of the clay particles. If SAD patterns were obtained from very small specimen areas as described above, however, *hkl* rows with discrete diffraction spots were obtained from some specimen areas (Figure 2c); such *hkl* rows are inconsistent with purely turbostratic stacking.

It is clear from the SAD experiments described here that the diffraction pattern obtained depended strongly on how the experiment was done. Normal SAD technique yielded patterns that can be interpreted in terms of turbostratic stacking. If experimental technique and optics were such that SAD patterns were obtained from more limited areas, however, the same specimen yielded patterns indicative of coherent layer stacking. These contrasting results suggest that the turbostratic patterns were produced simply by averaging over an aggregation of numerous coherently stacked crystallites that were randomly oriented with respect to each other, rather than resulting from a truly turbostratic structure.

These results further show that caution must be exercised in the interpretation of turbostratic SAD patterns. A turbostratic ring pattern may, indeed, indicate that the stacking is fully turbostratic. Such a pattern also can be produced, however, by the overlapping of numerous, very thin crystallites that have internal coherent stacking.

Electron microscopy

Conventional TEM imaging. Low-magnification, bright-field images of ion-milled samples of both I/S specimens showed that they consisted of small, bent crystals or packets without consistent orientation. The

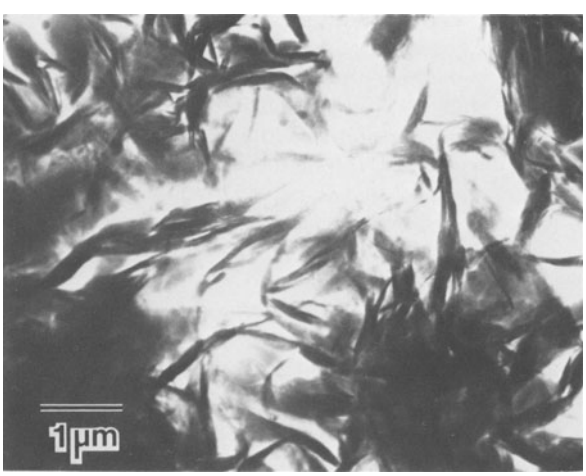


Figure 3. Transmission electron micrograph showing overview of I/S crystals in the R>1 sample and characteristic chaotic intergrowth, porosity, and bending of crystallites.

https://doi.org/10.1346/CCMN.1990.0380101 Published online by Cambridge University Press

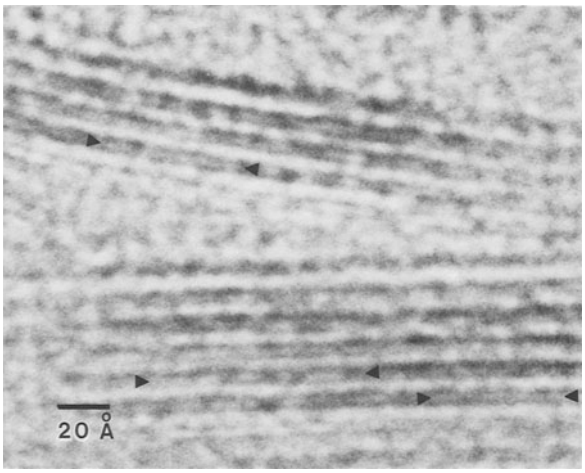


Figure 4. High-resolution transmission electron microscope image from R>1 sample, showing splitting of the dark fringe (arrowed) that occurs for well-oriented crystals near Scherzer focus (see Guthrie and Veblen, 1989b).

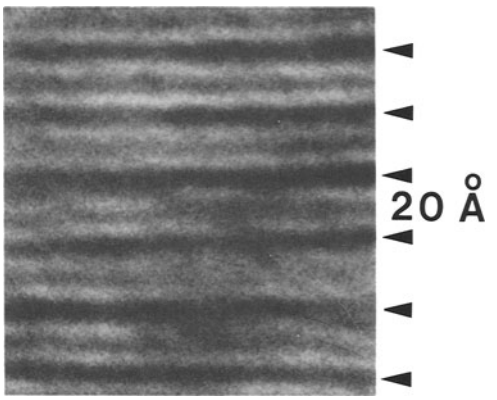


Figure 5. High-resolution transmission electron micrograph showing 2-layer ordering in the R1 sample. Computer simulations indicate that heavier dark fringes (arrowed) lie near positions of smectite interlayers. Spacing between heavy dark fringes is 20 Å. $\Delta f \simeq +1000$ Å.

texture had a somewhat ropy appearance (Figure 3), and substantial porosity was apparently present, although ion milling tends to enlarge holes in porous materials. As discussed above, the small crystal size and highly variable orientation due to bending of the crystallites made TEM work on these materials difficult. In addition to I/S, a very small amount of chlorite was found in the R1 specimen as discrete crystals a few hundred Ångströms thick. Although the chlorite probably represented less than 1% of the specimen, it was observed easily because it did not damage in the electron beam nearly so rapidly as did the I/S.

High-resolution TEM of layer sequences. Images obtained from both I/S specimens under HRTEM conditions typically showed major changes in image character across the area recorded on a film, a result of the fine-scale bending of the I/S seen in Figure 3. In addition, subgrains (crystals or packets of layers that locally have relatively uniform contrast and hence orientation) range in thickness from a few tens to a few hundreds of Ångströms, although some were larger.

The details in the HRTEM images showing only basal (00*l*) fringes (e.g., those obtained with an objective aperture that excluded *hkl* beams) were broadly consistent with the one-dimensional computer simulations presented by Guthrie and Veblen (1989a, 1989b, 1989c). For example, all such images showed light and dark fringes having spacings of about 10 Å. In underfocused images obtained at $\Delta f \simeq -1000$ Å, little or no contrast was noted that could be interpreted as resulting from the ordering of I and S layers. Inasmuch as these were the "optimum defocus" conditions that are typically used for obtaining HRTEM images, images obtained under the most usual operating conditions were apparently not appropriate for observing I/S mixed layering. In some underfocused images, the dark fringes were split in half by a narrow light fringe (Figure 4). The simulations suggest that images of this sort were obtained from parts of crystals that were close to perfect orientation in the electron microscope (i.e., with the electron beam parallel to the layers).

Images obtained under conditions of overfocus commonly showed modulations in the intensities of the fringes that were consistent with I/S ordering. Specifically, darker black fringes occurred in a pattern that suggested that they corresponded to smectite interlayers. The computer simulations confirm this interpretation, but they also show that the dark fringes did not necessarily overlie the interlayer positions exactly. In the R1 specimen, intense black fringes tended to alternate with black fringes that were less intense, indicating the sequence . . .ISIS. . . (Figure 5). In the R>1 specimen, the more intense black fringes commonly were separated by three less intense fringes (corresponding to a block having the structure SIIIS); however, the intense black smectite fringes also were commonly separated by 2, 4, 5, or more illite fringes. The Zempleni R>1 I/S thus does not appear to possess a perfectly ordered structure (Figure 6), although some regions obviously have sufficient 4-layer ordering to give rise to SAD patterns such as that in Figure 1b. Thicker regions of the specimens also produced images showing periodicities due to I/S ordering. Figure 7 is an overview of such an area having good R1 ordering; this illustration also shows that some of the layers bend or terminate, producing a somewhat ropy texture.

S/(S + I) ratios from HRTEM images

The fraction of smectite layers in an I/S crystal may be obtained directly from an overfocused HRTEM image that shows basal fringes corresponding to the I and S layers. In theory, this is done simply by counting the

https://doi.org/10.1346/CCMN.1990.0380101 Published online by Cambridge University Press

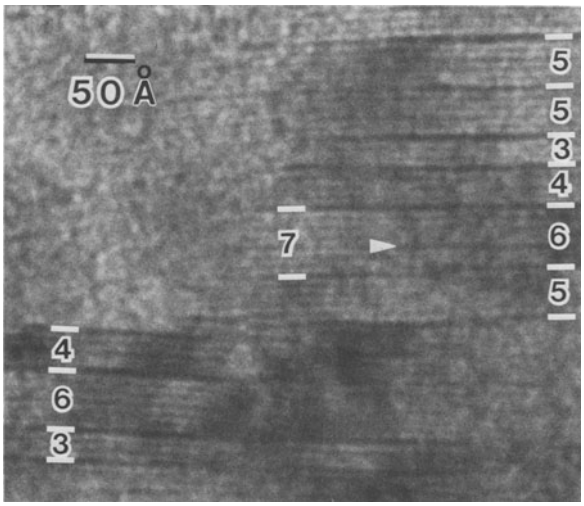


Figure 6. High-resolution transmission electron micrograph showing variable spacing between smectite interlayers in the R>1 sample. Dark fringes lie near smectite interlayers (Guthrie and Veblen, 1989a). Numbers refer to total number of 2:1 layers in each packet, i.e., the number of illite layers plus one. One smectite interlayer terminates, becoming an illite interlayer (arrowed). $\Delta f \simeq +1000$ Å.

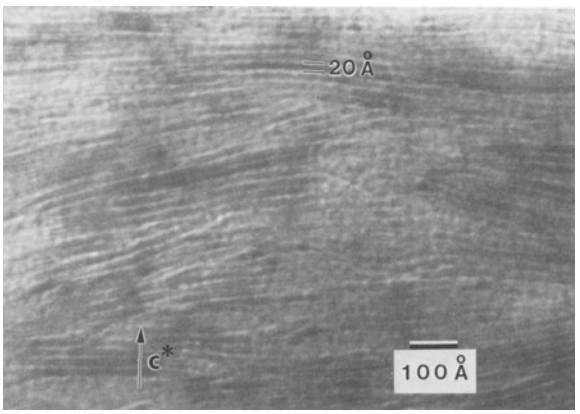


Figure 7. High-resolution transmission electron microscope image from a relatively thick part of R1 sample, showing 20-Å periodicity due to R1 ordering over an extended area. The c^* axis in one local region is indicated.

numbers of the layers and calculating the ratio S/(S + I). This ratio can then be compared with the smectite fraction obtained from XRD, as discussed below, to see if the two methods are consistent with each other.

In practice, counting I and S layers is not straightforward for many images, due to poor quality of the images and the fact that contrast from the I and S layers does not appear for all orientations, crystal thicknesses, etc. The decision on how dark a fringe must be to qualify as a smectite fringe is clearly subjective; however, in some images the distinction is obvious. Therefore, we took the approach of counting I and S layers only in parts of images where the ordering pattern was fairly obvious. Three different microscopists also obtained and interpreted the data independently on both the R1 and R>1 specimens. The two (001) bounding surfaces of the crystallites were counted as a single S layer.

The results of the counts of I and S layers are shown in Table 3. The S/(S + I) ratios obtained by the three microscopists are consistent, considering the relatively poor images that can be obtained from these experimentally difficult materials. The ratios obtained from the two specimens are within the ranges expected for R1 and R>1 I/S. Quantitative comparison with the ratios derived by XRD is addressed below.

Layer stacking and computer simulations of cross-fringe intensity

In addition to the basal fringes arising from the 00*l* reciprocal lattice row, many images showed 4.5-Å cross-fringes formed by imaging *hkl* rows; these fringes correspond to the (020) and (110) planes indexed in the simple $C2/m$ unit cell of 1*M* sheet silicates. This result is consistent with the work of Ahn and Buseck (1990), who obtained two-dimensional lattice images with an ultra-high-resolution instrument; indeed, one of the samples used by them was the Zempleni (R>1) material described here. In our study, depending on defocus conditions and slight variations in orientation, the cross-fringes occurred either alone or in combination with the basal fringes to form two-dimensional lattice images. To study the cross-fringes in detail, HRTEM experiments were made using an objective aperture matched to the point-to-point resolution of

Table 3. Smectite/(illite + smectite) [S/(I + S)] ratios obtained from high-resolution transmission electron microscopy (HRTEM) and X-ray powder diffraction (XRD).

HRTEM data	R1 sample			R>1 sample		
	S-layers	I-layers	S/(I + S)	S-layers	I-layers	S/(I + S)
Operator 1	281	283	0.50	116	431	0.21
Operator 2	349	425	0.45	80	187	0.30
Operator 3	183	230	0.44	39	91	0.30
Operators 1–3, totals	813	938	0.46	235	709	0.25
XRD	S/(I + S) = 0.45 = 45%			S/(I + S) = 0.17 = 17%		

https://doi.org/10.1346/CCMN.1990.0380101 Published online by Cambridge University Press

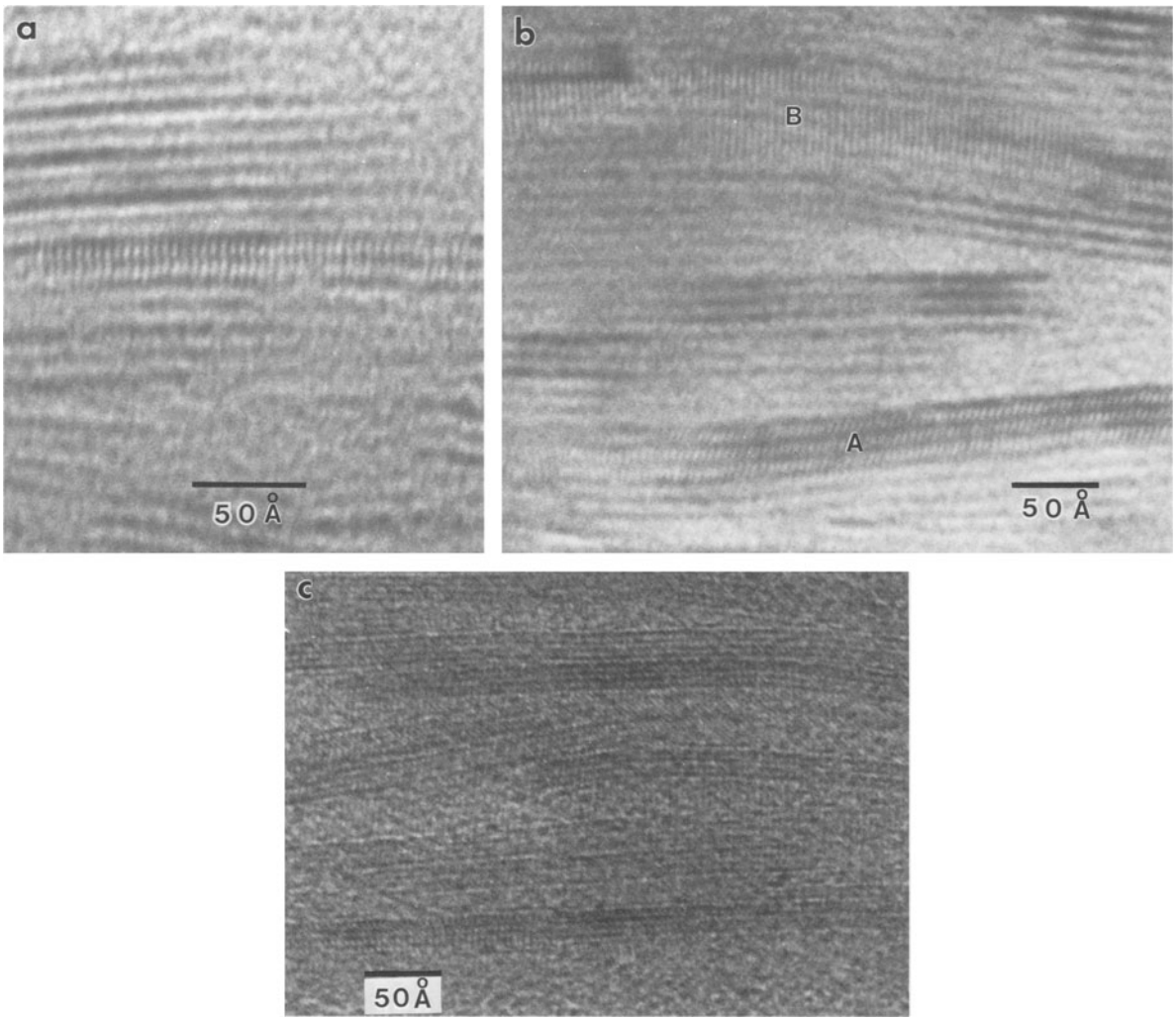


Figure 8. High-resolution transmission electron micrographs showing 4.5-Å cross-fringes. (a) Fringes crossing only two 2:1 layers in the R1 sample. (b) Fringes indicating coherent stacking of three layers (area A) and more layers (area B) in the R1 sample. (c) Large, coherently stacked crystal in the R>1 sample. Basal fringes are approximately horizontal, and cross-fringes are fine lines that cut across them in a vertical orientation.

the ST objective lens (3.0 Å), taking care to orient the sample region of interest with the layers approximately parallel to the electron beam. The sample was observed both at overfocus (to confirm that ordering of I/S layers was present in the area of interest) and at optimum underfocus conditions for imaging of the cross-fringes.

The implication of such cross-fringes is that the rotation of adjacent layers was not random, i.e., that the regions of I/S traversed by them were not turbostratic but instead were coherently stacked. Thus, the observation of cross-fringes is in agreement with the electron diffraction evidence showing that the stacking vectors were not randomly distributed from layer to layer. Instead, these fringes are consistent with the same layer rotations that occur in micas, i.e., 0°, ±60°, ±120°, and 180°.

The range of coherent stacking as evidenced by the extent of cross-fringes was only rarely on the scale of the fundamental particles. Figure 8a shows a two-dimensional lattice image having cross-fringes extending over only 20 Å in the R1 specimen, which is the thickness of the fundamental particles in this material; this image was obtained at overfocus and also shows basal fringe modulations due to R1 I/S ordering. The two-layer unit showing the cross-fringes is centered on an illite interlayer, as would be expected for the typical R1 fundamental particle as described by Nadeau *et al.* (1984a, 1984b, 1984c); however, this figure shows the only example we observed in which the range of cross-fringes was this short. More typically, the cross-fringes extended over at least several (but fewer than ten) 2:1 layers, as shown in Figure 8b, although some coher-

https://doi.org/10.1346/CCMN.1990.0380101 Published online by Cambridge University Press

ently stacked regions were substantially thicker than 100 Å (Figure 8c). These observations show that coherent stacking existed not only across illite (nonexpandable) interlayers, but also across smectite (expandable) interlayers.

To confirm rigorously that the observed cross-fringes imply mica-like, coherent stacking relations between the layers they cross, dynamical electron diffraction and image simulations were made, in which the intensities of the cross-fringes were calculated as a function of layer orientation with respect to the electron beam. The calculations were performed with the SHRLI programs (O'Keefe, 1984, as described by Guthrie and Veblen, 1989a), assuming that the (001) surfaces of adjacent layers were parallel to each other and to the electron beam.

Figure 9 compares the intensity profiles of the (010) fringes that arise if the beam is perfectly parallel to [100] (tilt = 0.0°) and if the crystal is rotated out of this orientation by increments of ~2° around c^*. Thus, at tilt = 0.0, the crystal is in perfect orientation for imaging the 4.5-Å cross-fringes, whereas in the other parts of Figure 9 the 4.5-Å planes are tilted by varying degrees with respect to the electron beam. The calculations show that layer rotations of only about 2° would produce major changes in fringe contrast from layer to layer. For example, almost a twofold change in contrast existed between 0° and 2.1°, and some orientations (e.g., 6.4° and 10.7°) produced contrast low enough that it probably would not have been observed on film.

These image calculations confirm that random rotations between layers (i.e., turbostratic stacking) would have produced major modulations in the cross-fringe intensities. The contrast of the observed cross-fringes, however, showed no such variations. Therefore, the range of coherent stacking typically extended for distances substantially larger than the fundamental particle thickness. Thus, on the HRTEM scale of observation, the two I/S specimens are not turbostratic.

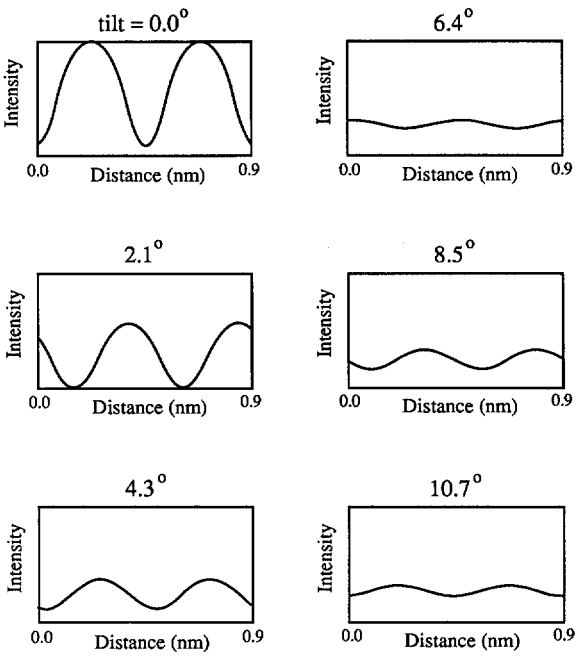


Figure 9. Computer-simulated intensity profiles for the 0k0 cross-fringes in high-resolution transmission electron micrographs as a function of the angle of rotation away from the a-axis around c^*. 0° profile refers to fringes produced if beam is aligned perfectly parallel to the a-axis. Even minor layer rotations of ~2° would produce major changes from layer to layer in the cross-fringe intensity profiles.

DISCUSSION AND CONCLUSIONS

The HRTEM observations on mixed-layer I/S are consistent with the computer simulations of HRTEM images reported by Guthrie and Veblen (1989a, 1989b, 1989c). Although the imaging of the layer sequences in I/S was experimentally difficult, exact sequences and the ratios of I and S layers were derived from the better quality images. The results on the R1 and R>1 I/S obtained with both X-ray powder diffraction and HRTEM are compared below, the structural state of I/S as it occurs in the natural specimens (i.e., prior to preparation for XRD analysis) is discussed in light of the electron diffraction and imaging studies, and how these observations are related to the fundamental particle hypothesis is considered.

Comparison of XRD and HRTEM results on layer stacking

The results presented in Table 3 show that all three TEM operators obtained similar S/(I + S) ratios by counting layers in HRTEM images. Thus, the layer ratios characteristic of R1 and R>1 ordering clearly can be distinguished in this way, at least by experienced operators and using the methodology outlined above.

Pooling the layer counts of all three operators gives an overall S/(I + S) ratio obtained for the R1 sample of 0.46 (i.e., 46%), whereas for the R>1 sample, the ratio is 0.25 (i.e., 25%). These values are similar to values determined by XRD of 45% and 17%, respectively. Given the sampling and counting errors associated with the HRTEM data and the errors inherent in XRD determinations of such ratios, the agreement is remarkably good. Even apparent differences in the HRTEM determinations of the three operators (21%, 30%, 30%) can be largely accounted for by counting statistics alone, not to mention other sampling errors and variations due to differences in techniques used by the different operators. Furthermore, the relatively minor difference between the HRTEM and XRD data for the R>1 specimen may have resulted from the way the HRTEM data were compiled. If relatively large patches of I/S were encountered that contained no dark

https://doi.org/10.1346/CCMN.1990.0380101 Published online by Cambridge University Press

fringes that could be attributed to smectite layers, the region was assumed to be in improper orientation for the ordering to be observed. Some of these areas, however, may have been regions of pure illite, and counting them as such would have lowered the S/(S + I) ratio and produced better agreement with the XRD results.

The data in Table 3 therefore suggest that the HRTEM images and the XRD data measured the same structural characteristic in I/S. The XRD data suggest many sequences of the type . . .ISIS. . . in the R1 sample and many sequences in which S layers were separated by several I layers in the R > 1 material. Indeed, even qualitative analysis of the HRTEM data supports this suggestion: images of the R1 sample showed many areas in which . . .ISIS. . . ordering was perfect over dozens of repeats, whereas the R > 1 sample tended to have many regions similar to that shown in Figure 6, containing more than one I layer between pairs of S layers.

Structural state of illite/smectite

Layer sequence. The structure of mixed-layer clays, especially that of I/S, has been greatly discussed. Much of the recent discussion has been prompted by the reports of Nadeau *et al.* (1984a, 1984b, 1984c), which include the observation that mixed-layer I/S clays deposited from suspensions (e.g., on XRD mounts) commonly consist of populations of "fundamental particles," only one to a few layers thick. From this observation, Nadeau and coworkers have inferred that the "smectite" layers observed by XRD correspond to the expandable interfaces between adjacent particles.

These observations may simply imply that I/S separates along the smectite interlayers during preparation for XRD, producing the thin fundamental particles. If the suspension dries, the particles reassemble and collapse together well enough that they produce XRD patterns indicative of periodic structures by "interparticle diffraction." Some mineralogists, however, have interpreted the conclusions of Nadeau *et al.* (1984a, 1984b, 1984c) to suggest that I/S does not exist as discrete, identifiable crystals (see, e.g., discussion by Mackinnon, 1987). In this view, the ordered I/S layer sequences observed in XRD experiments are merely an artefact of the X-ray specimen preparation procedure, and the apparent ordering is not related to the layer sequence of I/S as it occurs in the bulk, untreated specimen. Prior to the reinterpretation of Ahn and Peacor (1989), such a view was perhaps useful for explaining why no ordering was found in electron microscopy studies of clays that appear ordered in XRD experiments (e.g., Ahn and Peacor, 1986a). As argued by Mackinnon (1987), however, previous HRTEM studies tended to suggest that regular layer sequences can occur as coherent domains. This view also is supported by the work and discussion of Ahn and Peacor (1986b) on rectorite.

Our computer simulations and experimental results help to resolve the question of the initial structural state of I/S. For the two specimens studied here, SAD and HRTEM experiments showed that both R1 and R > 1 layer sequences can exist in the bulk material. These ordering schemes therefore are not merely an artefact of preparation for XRD experiments. The layer sequence observed by XRD reflects the one-dimensional sequence of layers present in the original, bulk specimen, and both HRTEM and XRD experiments can provide information on the primary proportion of smectite (expandable) layers that existed in the I/S prior to treatment for XRD. This conclusion is in agreement with the recent work of Środoń *et al.* (1990), who used the thicknesses of treated, uncollapsed I/S packets to show similar S/(S + I) ratios in HRTEM and XRD specimens. It also agrees with the very high-resolution TEM study of Ahn and Buseck (1990), who showed that the range of coherent stacking exceeds the size of the fundamental particles. Finally, our results are consistent with the ^{29}Si nuclear magnetic resonance study of Altaner *et al.* (1988), which suggested that the surfaces of fundamental particles are smectitic.

Although XRD experiments apparently provide information on the initial I/S layer sequences, the crystals do not necessarily remain intact through the sample preparation. No doubt they separate along many, if not all, of their smectite interlayers (i.e., the crystals disaggregate and turn into the fundamental particles of Nadeau *et al.*, 1984a, 1984b, 1984c), as suggested by Ahn and Peacor (1986a). If they reaggregate on drying, however, the numbers of I and S interlayers are essentially unchanged compared with those of the initial bulk specimen. Furthermore, if no separation occurs along illite interlayers, even the statistical distribution of the numbers of adjacent illite layers is preserved. Thus, the layer sequence is rearranged during specimen preparation, but the XRD experiment can still be used to determine the initial proportion of smectite layers and the statistical distribution of illite packets of various thicknesses.

Layer stacking. The SAD data, the presence of 4.5-Å cross-fringes that are continuous across a number of layers in HRTEM images, and computer simulations of these cross-fringe intensities show that the layer stacking in the two investigated samples was not turbostratic on the scale observable with HRTEM. Instead, the regions of coherent stacking (relative layer rotations of mod 60°) tend to extend over several layers, commonly encompassing several fundamental particles as defined by Nadeau *et al.* (1984b). The implications of this observation for the fundamental particle hypothesis are discussed below.

It is difficult to assess the degree of agreement between our HRTEM results indicating coherent layer stacking, at least over a short range, and those obtained

https://doi.org/10.1346/CCMN.1990.0380101 Published online by Cambridge University Press

with XRD methods. Diffuse *hk* bands in powder XRD patterns certainly indicate imperfect stacking, but a systematic and rigorous attempt has not yet been made to quantify the degree and exact form of line broadening, which may turn out to be consistent either with coherent stacking disorder and the shape effect for very small crystalline or with pure turbostratic stacking.

Even if XRD experiments on dispersed and sedimented samples eventually suggest that I/S is perfectly turbostratic, this apparent discrepancy with the HRTEM data could result from the sample preparation methods used for XRD studies; as noted above, the fundamental particles may become fully disaggregated, and the XRD sample may be turbostratic regardless of the initial stacking state. Studies of some materials, however, apparently show the same degree of diffuseness in the XRD pattern prior to dispersion of the sample (Méring and Oberlin, 1971). For such materials, it is possible that the clay was initially turbostratic and remained so, that the material was not fully disaggregated in the sedimented XRD mount, or even that fundamental particles reoriented themselves (i.e., recrystallized) during sedimentation onto the XRD mount. Another consideration is that coherent stacking on the scale we have observed simply may be difficult to recognize in an XRD experiment. As noted above, most coherently stacked crystallites in our samples were fewer than ten 2:1 layers thick, and variations in cross-fringe direction indicated that these possessed non-turbostratic (coherent) stacking disorder. The diffuse diffraction due to this stacking disorder and the shape effect of the very thin, <100-Å crystals suggest that the coherent stacking will be difficult to recognize by XRD, even in undispersed samples. Future detailed XRD experiments, combined with computer simulation of XRD patterns for various degrees of stacking disorder and crystallite thickness, should help to resolve the question of how the XRD and HRTEM results on stacking are related to each other.

Note that our results cannot be generalized to all mixed-layer materials that have been called illite/smectite. We have studied only two relatively well-ordered specimens of hydrothermal potassium I/S. Possibly I/S occurs in some rocks as isolated, fundamental particles, as it surely must in many natural aqueous suspensions. It is also possible that it can occur with only one-dimensional order, as completely turbostratic assemblies of particles; this is more likely in I/S samples with Na, for example, as the predominant interlayer cation, rather than K. In fact, an entire range of ordering states probably exists in natural I/S. We have shown, however, that at least some I/S possesses coherent, non-turbostratic stacking that extends across the fundamental particles of Nadeau and coworkers.

Definition of "fundamental particles" and their interactions. The above findings present a problem of nomenclature, because Nadeau *et al.* (1984b) *defined* fundamental particles "as individual or free particles that yield single-crystal electron diffraction patterns from the *ab* plane." It is not clear in this definition exactly what is meant by an "individual" particle, but it is now very clear that the particles of Nadeau *et al.* (1984a, 1984b, 1984c) are not "free" in the original, untreated specimen, at least in the materials we have studied. Not only does the I/S possess ordered arrangements of I and S layers (or nonexpandable and expandable layers) prior to disaggregation, but it also possesses non-turbostratic coherence of stacking across the fundamental particles, at least for short distances.

Therefore, if the term "fundamental particle" is to be used for all mixed-layer I/S as it occurs in nature, its definition must be altered to include particles that are not free. Furthermore, because there is crystallographic coherence across many (but not all) of the fundamental particle boundaries, these particles probably possess a non-trivial thermodynamic interaction with adjacent particles. Indeed, given their layer sequences and mica-like stacking, the coherently stacked packets of fundamental particles we observed should be called crystals (or crystallites, to indicate their small size). Of course, they are very disordered crystals, but virtually all crystals possess some degree of disorder (e.g., Veblen, 1985a, 1985b), and disorder is recognized by crystallographers as an essential trait of naturally occurring crystals (Schock, 1985).

An appropriate thermodynamic description of the samples described in this paper could be formulated in at least three ways. First, the particles of Nadeau and coworkers could be treated as the fundamental units, but here at least two different types of boundaries must be considered between these units (coherently stacked and turbostratic). The more normal treatment for crystalline materials also would be appropriate. A free energy term could be assigned to ideal, bulk crystalline I/S, with very important modifying energy terms for the state of disorder and the very large surface area per unit volume. This treatment would be analogous to the usual thermodynamic treatment that takes account of the surface free energy for small particles (e.g., Enüstün and Turkevich, 1960). Finally, I/S might be treated as two separate phases (illite and smectite), in the fashion of Altaner *et al.* (1988).

This discussion should not be taken to imply that the concept of fundamental particles is not useful, simply because they can occur in coherently stacked crystallites and presumably interact energetically. Indeed, similar structural modules are used extensively when dealing with complex structures (e.g., Thompson, 1978). Guthrie and Veblen (1989c) used layer modules to formulate atomic positions of many mixed-layer silicates in order to simulate their HRTEM images. For the fundamental particle concept for I/S, the utility of such modules is even greater than for most minerals, be-

https://doi.org/10.1346/CCMN.1990.0380101 Published online by Cambridge University Press

cause mixed-layer clays can be physically disassembled into their constituent modules, unlike most silicates. The fundamental particle concept therefore provides a useful language for addressing the physical and chemical interactions of mixed-layer materials, and it is a useful device for explaining the significance of long-range stacking order along c^* ($R>1$).

Future role of TEM methods in studies of I/S

In this and our companion papers (Guthrie and Veblen, 1989a, 1989b, 1989c), we have shown that layer sequences in I/S and the range of coherent stacking can be imaged with HRTEM and studied with electron diffraction. We have shown theoretically how such imaging can be performed and demonstrated that even electron microscopes of moderate resolution are optically capable of this type of work. The specimen preparation, however, is difficult; the I/S damages rapidly in the electron beam, and the small crystal size and the fact that the crystals are bent preclude normal microscopy procedures for specimen orientation. All of these factors make the microscopy much less routine and more frustrating than it is for normal minerals, and the final result is images that have low contrast, are difficult to interpret, and are not nearly so visually appealing as HRTEM images of many other structures.

On the other hand, the combination of HRTEM and electron diffraction can provide information that to date has not been obtainable in any other way. Future studies on other specimens should resolve further the question of the structural state of I/S as it occurs prior to treatment for XRD analysis. XRD, however, is a relatively rapid, well-established tool for the study of mixed-layer clays, and it is applied routinely in numerous laboratories worldwide. Our results suggest that XRD methods can provide an accurate picture of the average structure of I/S. Although further HRTEM studies should be carried out on I/S, HRTEM is not likely to replace XRD as the standard structural probe for mixed-layer clays.

Another future use of HRTEM data on mixed-layer I/S will no doubt be in the analysis of the exact sequences of I and S layers. In this paper we have limited the discussion to the bulk ratios of I and S layers; however, the raw data are in the form of I/S sequences, and these could be compared directly with sequences inferred from XRD methods. In the past few years, there has been a high level of interest in the thicknesses of I/S particles, and the problem has been addressed theoretically, in terms of Ostwald ripening theory, with XRD experiments, and as a way of examining the reactions by which smectite transforms to illite (e.g., Altaner and Bethke, 1988; Eberl and Środoń, 1988; Inoue *et al.*, 1988). Future work may combine HRTEM and XRD to assess critically the assumptions and conclusions of such studies.

ACKNOWLEDGMENTS

We appreciate useful discussions with Mark DiStefano, Jillian Banfield, Peter Heaney, and Eugene Ilton. The paper benefited immensely from a thorough review by and discussion with Paul Nadeau, as well as from an anonymous review. We thank Michael O'Keefe for providing the diffraction and image simulation software and Wayne Rasband for the program IMAGE, which was used to analyze computed image intensities. Samples were kindly supplied by Atsuyuki Inoue and Jan Środoń. This research was supported by Conoco, Inc. and NSF grants EAR86-09277 and EAR89-03630. TEM work was performed at the Johns Hopkins high-resolution electron microscopy laboratory, which was established with partial support from NSF grant EAR83-00365.

REFERENCES

Ahn, J. H. and Buseck, P. R. (1990) Layer-stacking sequences and structural disorder in mixed-layer illite/smectite: Image simulations and HRTEM imaging: *Amer. Mineral.* **75,** (in press).

Ahn, J. H. and Peacor, D. R. (1986a) Transmission and analytical electron microscopy of the smectite-to-illite transition: *Clays & Clay Minerals* **34,** 165–179.

Ahn, J. H. and Peacor, D. R. (1986b) Transmission electron microscope data for rectorite: Implications for the origin and structure of "fundamental particles": *Clays & Clay Minerals* **34,** 180–186.

Ahn, J. H. and Peacor, D. R. (1989) Mixed-layer illite/smectite from Gulf Coast shales: A reappraisal of TEM images: *Clays & Clay Minerals* **37,** (in press).

Altaner, S. P. and Bethke, C. M. (1988) Interlayer order in illite/smectite: *Amer. Mineral.* **73,** 766–774.

Altaner, S. P., Weiss, C. A., Jr., and Kirkpatrick, R. J. (1988) Evidence from ^{29}Si NMR for the structure of mixed-layer illite/smectite clay minerals: *Nature* **331,** 699–702.

Eberl, D. D. and Środoń, J. (1988) Ostwald ripening and interparticle-diffraction effects for illite crystals: *Amer. Mineral.* **73,** 1335–1345.

Enüstün, B. V. and Turkevich, J. (1960) Solubility of fine particles of strontium sulfate: *J. American Chem. Soc.* **82,** 4502–4509.

Guthrie, G. D., Jr. and Veblen, D. R. (1988) Simulated high-resolution transmission electron microscope images of mixed-layer illite/smectite clays: in *Prog. and Abstracts, The Geochemical Society V. M. Goldschmidt Conf.,* p. 45.

Guthrie, G. D., Jr. and Veblen, D. R. (1989a) High-resolution transmission electron microscopy of mixed-layer illite/smectite: Computer simulations: *Clays & Clay Minerals* **37,** 1–11.

Guthrie, G. D., Jr. and Veblen, D. R. (1989b) High-resolution transmission electron microscopy applied to clay minerals: in *Spectroscopic Characterization of Minerals and their Surfaces,* L. M. Coyne, D. F. Blake, and S. McKeever, eds., American Chemical Society Symposium Series No. 415, 75–93.

Guthrie, G. D., Jr. and Veblen, D. R. (1989c) Interpreting one-dimensional high-resolution transmission electron micrographs of sheet silicates by computer simulation: *Amer. Mineral.* **74,** (in press).

Hirsch, P., Howie, A., Nicholson, R. B., Pashley, D. W., and Whelan, M. J. (1977) *Electron Microscopy of Thin Crystals*: 2nd ed., Robert E. Krieger Publishing Company, Malabar, Florida, 563 pp.

https://doi.org/10.1346/CCMN.1990.0380101 Published online by Cambridge University Press

Inoue, A., Minato, H., and Utada, M. (1978) Mineralogical properties and occurrence of illite/montmorillonite mixed layer minerals from Miocene volcanic glass in Waga-Omono district: *Clay Sci.* **5,** 123–136.

Inoue, A. and Utada, M. (1983) Further investigations of a conversion series of dioctahedral mica/smectites in the Shinzan hydrothermal alteration area, northeast Japan: *Clays & Clay Minerals* **31,** 401–412.

Inoue, A., Velde, B., Meunier, A., and Touchard, G. (1988) Mechanism of illite formation during smectite-to-illite conversion in a hydrothermal system: *Amer. Mineral.* **73,** 1325–1334.

Keller, W. D., Reynolds, R. C., and Inoue, A. (1986) Morphology of clay minerals in the smectite-to-illite conversion series by scanning electron microscopy: *Clays & Clay Minerals* **34,** 187–197.

Livi, K. J. T. and Veblen, D. R. (1987) "Eastonite" from Easton, Pennsylvania: A mixture of phlogopite and a new form of serpentine: *Amer. Mineral.* **72,** 113–125.

Mackinnon, I. D. R. (1987) The fundamental nature of illite/smectite mixed-layer clay particles: A comment on papers by P. H. Nadeau and coworkers: *Clays & Clay Minerals* **35,** 74–76.

Méring, J. and Oberlin, A. (1971) The smectites: in *The Electron Optical-Investigation of Clays,* J. A. Gard, ed., Mineralogical Society, London, 193–229.

Nadeau, P. H. (1985) The physical dimensions of fundamental clay particles: *Clay Miner.* **20,** 499–514.

Nadeau, P. H., Wilson, M. J., McHardy, W. J., and Tait, J. M. (1984a) Interstratified XRD characteristics of physical mixtures of elementary clay particles: *Clay Miner.* **19,** 67–76.

Nadeau, P. H., Wilson, M. J., McHardy, W. J., and Tait, J. M. (1984b) Interparticle diffraction: A new concept for interstratified clays: *Clay Miner.* **19,** 757–769.

Nadeau, P. H., Wilson, M. J., McHardy, W. J., and Tait, J. M. (1984c) Interstratified clays as fundamental particles: *Science* **225,** 923–925.

O'Keefe, M. A. (1984) Electron image simulation: A complementary image processing technique: in *Electron Optical Systems,* AMF O'Hare, Chicago, 209–220.

Schock, R. N., ed. (1985) *Point Defects in Minerals: Geophysical Monograph* **31,** American Geophysical Union, Washington, D.C., 232 pp.

Środoń, J., Andreoli, C., Elsass, F., and Robert, M. (1990) Direct HRTEM measurement of expandability of mixed-layer illite/smectite in bentonite rock: *Clays & Clay Minerals* **38,** (in press).

Thompson, J. B., Jr. (1978) Biopyriboles and polysomatic series: *Amer. Mineral.* **63,** 239–249.

Veblen, D. R. (1985a) Extended defects and vacancy nonstoichiometry in rock-forming minerals: in *Point Defects in Minerals, Geophysical Monograph* **31,** R. N. Schock, ed., American Geophysical Union, Washington, D.C., 122–131.

Veblen, D. R. (1985b) Direct TEM imaging of complex structures and defects in silicates: *Annual Review Earth Planetary Sci.* **13,** 119–146.

(Received 30 January 1989; accepted 13 August 1989; Ms. 1877)

https://doi.org/10.1346/CCMN.1990.0380101 Published online by Cambridge University Press